Ultrasonic and Impact-Echo Testing for the Detection of Scaling in Geothermal Pipelines

Isabelle Stüwe[1] · Lilly Zacherl[2] · Christian U. Grosse[1]

© The Author(s) 2023

Abstract

The efficiency and longevity of components in geothermal plants are significantly reduced by mineral deposition in pipes, also known as scaling [1]. A number of methods are used to monitor fouling (a broader term for all types of organic and inorganic deposition) in other industries, such as the oil, gas and food industries. These include direct and indirect, offline, in-situ and online, as well as inline methods, each of which have pros and cons [2,3]. An effective monitoring solution specific to the high temperature conditions in geothermal plants, which optimises maintenance and cleaning measures in dependency of scaling, has yet to be developed. In this paper, two non-destructive testing techniques: contact ultrasonic testing (UT) and impact-echo (IE) testing are investigated in their viability as methods to detect scaling growth in geothermal plants. A descaling measurement was conducted on a heavily scaled segment of an obsolete pipeline from the production well of the geothermal power plant in Sauerlach, Germany. The pipeline segment was inserted in a test rig and the scaling was gradually etched away using an acidic solution. At regular time intervals, the scaling thickness was measured mechanically and contact UT as well as IE measurements were carried out. The testing apparatus was designed to withstand high temperatures (140 °C at the inlet pipe surface) and to be easy to install whilst being cost-efficient. Both techniques yielded usable results with submillimeter resolution. The advantages and limitations of the two methods are discussed. Impact-echo testing, in particular, can be automated and presents a simple and cost-efficient scaling monitoring option.

Keywords Ultrasonic testing · Impact-echo · Scaling · Geothermal plants · High temperature

1 Introduction

With the increasing tendency toward renewable energy, geothermal plants are a growing industry [1–3]. From 1995 to 2005 a worldwide increase in geothermal energy production from 112441 to 587786.4 TJ/year was documented by the international geothermal association (IGA) [4]. The German geothermal association (BVG) lists a total of 38 running geothermal plants, 4 plants under construction and a further 30 plants planned in Germany.

Scaling presents a major cause for loss of efficiency and part failure (such as in heat exchangers or pumps). Whilst a number of monitoring concepts are used to detect scaling in other industries, an effective scaling monitoring solution for the high temperature conditions in geothermal plants does not yet exist. Most often, scaling in geothermal plants is addressed with regular cleaning measures using high doses of aggressive chemicals with limited knowledge of the present degree of scaling [5].

In the oil and gas industries, offline methods commonly used to detect scaling include chemical analysis of the produced water or brine, and monitoring residual scaling inhibitor or the total suspended solids present. Whilst cost-effective and readily available, these indirect methods are limited in their accuracy as samples taken are not necessarily representative of the overall state of the pipeline and can deteriorate by the time they reach the lab [3]. In-situ and online techniques such as the Thickness Shear Mode Res-

✉ Isabelle Stüwe
isabelle.stuewe@tum.de

Lilly Zacherl
lilly.zacherl@tum.de

Christian U. Grosse
grosse@tum.de

1 Chair of NDT, Technical University of Munich, Franz-Langinger-Straße 10, 81245 Munich, Bavaria, Germany

2 Chair of Hydrogeology, Technical University of Munich, Arcisstr. 21, 80333 Munich, Bavaria, Germany

onator (TSMR) or the fiber optic detection principle require sensors to be inserted into the pipe and then measure scaling growth locally on the instrumentation itself [6,7]. TSMR measures the change in resonance frequency of a piezoelectric mass sensor due to the mass of the adherent scaling. The fiber optic detection system measures radiation transmitted through an optical fiber with a partially exposed core, whereby a reduction thereof would imply scaling growth on the fiber surface. For geothermal power plants in particular, a noninvasive approach would be favourable as the high temperature and large volume flow rate would require very robust instrumentation and careful calibration leading to down time. Pipeline Inspection Gauges (PIGS) can be used for inline inspection of pipelines and can map their inside geometry to determine scaling thickness [8]. A PIG which is adapted to the high temperature of geothermal water would, however, present quite a challenge. Scaling can also be detected indirectly by calculating the fouling resistance via temperature and flow rate measurements [9] or monitoring the pressure drop at the inlet and outlet of heat exchangers [10]. These methods are, however, insensitive to submillimeter fouling layers, can have a considerable error ($\pm$ 20%) and the measured phenomena are not exclusively caused by scaling, so results could be misinterpreted [3,9].

The aim of this research is to develop a practicable monitoring solution which optimises the administration of cleaning measures in geothermal plants in dependency of the amount of scaling present. To this end, two potential non-destructive techniques are investigated and discussed: UT and IE.

In standard contact UT, piezoelectric sensors are used to transmit ultrasound pulses into the test piece and record any reflected echoes. Two challenges for contact UT in this application are the high temperature and curved surface of geothermal pipes. Whilst there are a number of piezoelectric materials around [11], with sufficiently high Curie temperatures (beyond which they are depolarised, losing their piezoelectric properties) which could be tailor-made to fit a given curvature radius, the simpler and much less costly option is to place a temperature-resistant wedge between a standard contact transducer and the pipe surface. In a prototype version of IE testing, the response of the pipeline system to a manually applied impact using an impact hammer is measured using a lower frequency force sensor coupled directly to the pipe. The recorded signal is then analysed in the frequency domain [12].

The predominant type of scaling in the Bavarian Molasse basin, where the Sauerlach facilities are located, is calcite [2]. The research described in the following therefore focuses on this locally most common pipe-scaling combination of steel-calcite.

2 Experimental Setup

Scaling growth generally takes a considerable amount of time. For the purpose of our experiments, the time span in question, even using measures to accelerate the process, was unfeasible. A new 'top-down' rather than 'bottom-up' approach was devised in which existing heavily scaled pipeline segments were gradually descaled using an acidic solution. During the descaling process, ultrasound and impact-echo measurements were carried out. A descaling test rig was designed with the project partners Z & H Wassertechnik, measX, the Chair of Hydrogeology and the Chair of Non-Destructive Testing, Technical University of Munich, assembled by Z & H Wassertechnik and modified by TUM ZfP. The test rig and the two measurement techniques applied in the descaling experiment are described in this section.

2.1 Descaling Test Rig

The descaling test rig was designed to gradually descale a piece of heavily scaled pipe by pumping an acidic solution through it. A scaled pipe segment is clamped between two 4 cm thick plastic plates, with an inlet in the lower plate and an outlet in the upper plate, standing in a chemical-resistant glass fibre reinforced polymer (GFRP) tub with an outlet leading to a pump. The acidic solution used to etch away the scaling was the cleaning agent RS 990 by Z & H Wassertechnik GmbH, St. Wendel, with active components 50% nitric acid and 85% phosphoric acid. 20 L of RS 990 were diluted with desalinated water to a 50% solution, filled into the GFRP tub and circulated through the pipe segment via the pump. The course of the acidic solution through the test rig is shown by the arrows in Fig. 1a.

The test piece was a 30 cm piece of DN200 black steel pipeline with a wall thickness of 11.5 mm from the production well at the geothermal power plant in Sauerlach, Germany. The pipe had grown a $\sim$ 6.6 mm-thick scaling layer over the course of 6 months. The rate of scaling growth is highly dependent on factors such as how often the submersible pump in the production well is switched off and on. A cross section of the pipe with the initial scaling layer is shown in Fig. 1b at the top. A microscope image of a fine-cut scaling sample is shown in Fig. 1b bottom. The applicability of the methods described to other types of scaling is currently under investigation.

2.2 Contact Ultrasonic Testing Setup

Two factors which need to be considered in coupling contact ultrasound transducers to geothermal pipelines are the high temperature ($\sim$ 140 °C at the production well in Sauerlach) and the curvature of the surface. In the following measurement, a 2.7 cm-thick temperature-resistant polyphenylen-

Fig. 1 **a** Descaling test rig. An acidic solution was pumped in the direction of the arrows shown, through the pipe segment, gradually etching away the scaling layer. **b** Top: Cross section of scaling layer in the pipe segment. Bottom: Microscope image of a fine-cut scaling sample
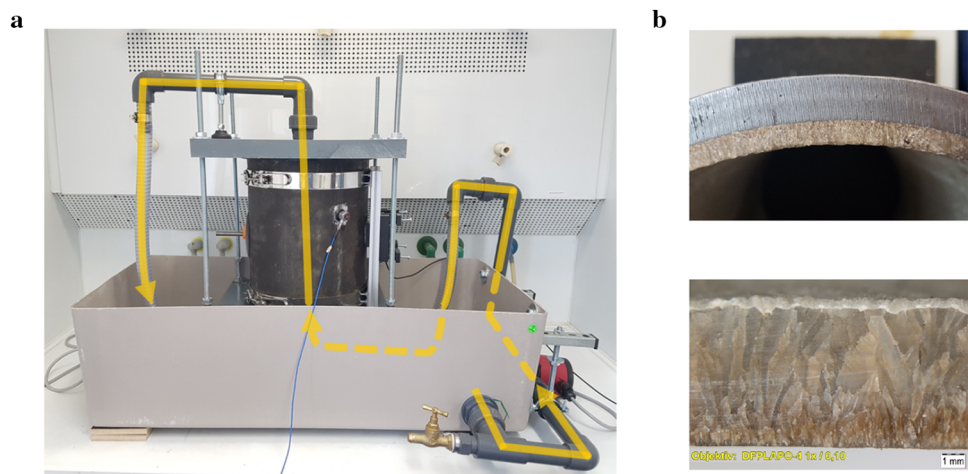
sulphon (PPSU) wedge, milled to fit the curvature of the pipe in the test rig, was used. Heat transfer through the PPSU wedge was tested by placing it on a sand bath (for even temperature distribution) on a hotplate at 150 °C for 15 h.

A high temperature couplant (Echotrace HT, Karl Deutsch) was used between probe and wedge and between wedge and steel pipe. A constant contact pressure was ensured by a combination of a suitably designed and 3D printed holding bracket and an elastic band (Fig. 2). Preliminary experiments comparing the signals recorded on pipe segments with and without scaling for a range of frequencies (0.5 MHz, 1 MHz, 2.25 MHz, 5 MHz, 10 MHz and 15 MHz) showed that 5 MHz was a good compromise between ultrasound range and resolution.

The ultrasound instrumentation used was an Olympus Omniscan MX2 in impulse-echo mode with a 5 MHz, 6 mm diameter Olympus V201 RM contact transducer. The parameters were set to 100 V pulse excitation voltage, 49 dB gain, zero noise reduction, no averaging and no filter. Over the course of the descaling experiment a set of 100 A-scans was recorded every 3 min. Aligning such a set of A-scans to resemble a B-scan showed no relevant phase change in the signals over the recording period which was on the order of 2 s. A much lower number of A-scans, for example 10, would suffice for the same SNR in future measurements. Data analysis was carried out in Matlab: The 100 A-scans recorded at each time step were averaged, for improved signal to noise ratio (SNR), and the time value corresponding to the amplitude peak of the pipe backwall echo was subtracted from that of the scaling backwall echo giving the two-way travel-time (TWT) in the scaling itself. The results are detailed in Sect. 3.1.

2.3 Impact-Echo Setup

In addition to the US contact measurements, an impact-echo measurement was carried out at each 3 min time interval.

The pipe was impacted manually with a steel impact hammer, the resulting signal was recorded using a force sensor and the frequency response of the system was analysed. On the receiving end we used a TiePie USB oscilloscope, connected via a signal conditioner to a broadband force sensor (both PCB Piezotronics) with an upper frequency limit of 36 kHz. The TiePie multichannel oscilloscope software was used for data acquisition. The measurement parameters were set to a range of 200 mV, 2 MHz acquisition rate and 50 kS per recording, giving a frequency resolution of 20 Hz. In the first descaling measurement a $\varnothing$ 5 mm steel impact hammer was used for excitation. Because the peak resonant frequency was not consistent over the course of the descaling experiment we also measured with a $\varnothing$ 10 mm impact hammer during the second experiment. The diameter and therefore, mass of the tip influences the stimulated frequency spectrum, whereby a smaller diameter leads to a higher and broader frequency spectrum [13]. The $\varnothing$ 10 mm impact hammer diameter yielded promising results: A clear and continuous correlation between scaling thickness and the excited resonant frequencies is observed, whereby resonance frequencies decrease with scaling thickness in the pipe. The different frequency peaks can be attributed to the excited wave modes [14,15].

The scaling thickness was also measured mechanically, for reference, using a threaded rod with a pointer at one end, a rubber tip at the other end and a 360° protractor. One full rotation of the threaded rod corresponds to a depth change of 1.5 mm. The concept is shown in Fig. 3. The scaling thickness at the beginning of the experiment was measured with a caliper.

2.4 Solution Analysis

For mass balance and calculating the scaling thickness via the calcium ion concentration, samples of the solution were taken after 3, 9 and 15 min, then every 9 min until 105 min,

Fig. 2 3D-printed holding bracket mounted on a strut profile to press a 5 MHz UT probe against the pipe (left) with a schematic close-up of the holding bracket pressing the probe onto the wedge and pipe (right)

Impact-echo sensor

Elastic band

PPSU wedge

Holding bracket for 5 MHz probe
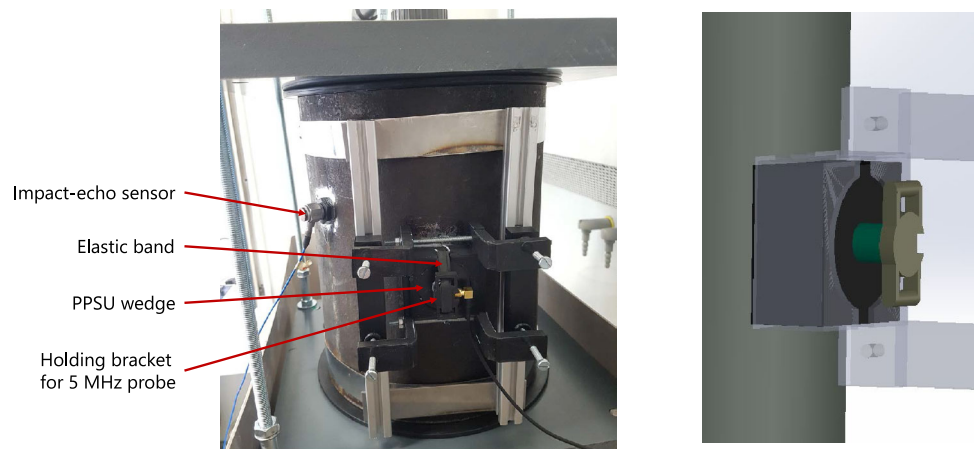
Fig. 3 Mechanical measurement of scaling thickness: The threaded rod is rotated until the rubber tip hits the scaling surface. The relative change in the number of rotations is recorded at each time interval

then every 30 min. The concentration of sodium, potassium, calcium and magnesium ions was determined by ion chromatography (IC; 881 Compact IC pro, Metrohm, Germany; column: C4-150, Metrohm, Germany). Before the measurement, the samples were diluted with ultra pure water (dilution factor of 500 and 1000 respectively) and filtrated (0.45 µm). The pH and EC of the solution were measured continuously with probes (Atlas Scientific, NY, USA) during the experiment.

3 Results

3.1 Results of Contact Ultrasound Measurement

The first contact US descaling measurement yielded a linear plot of scaling thickness against TWT. Once the relevant peaks were identified, the shift in their position could be tracked over the course of the measurement, revealing the scaling thickness inside the pipe. Figure 4 shows the averaged A-scans for two points in the measurement time series:

One was recorded near the beginning and one at the end of the first descaling measurement, corresponding to scaling thicknesses of 6.6 mm and 3.35 mm, respectively. The pipe and scaling backwall echoes are indicated.

The evolution of the TWT with scan time is shown in Fig. 5a and b for the first and second descaling measurement, respectively. The plateaus in the scatter plots shown are due to the limited time resolution of the instrumentation with the specified measurement parameters (0.05 µs). A higher resolution could be achieved using the described instrumentation by reducing the A-scan time frame. Whilst the pipe and scaling can easily be distinguished during the first measurement, the progressively thinner scaling layer thickness in the second descaling measurement makes superposition of the pipe and scaling backwall echoes a problem. A-scans in which the relevant backwall echoes could no longer be distinguished were removed in Fig. 5b. This included all A-scans taken after 69 min into the experiment, corresponding to a scaling thickness of $\sim$ 1.5 mm.

The travel time plotted against scaling thickness for the first and second measurements is shown in Fig. 6. The mechanically measured scaling thickness had a considerable error of $\pm$ 0.4 mm ($\pm$ 0.16 mm due to acid corrosion of the threaded hole in the steel pipe over the course of the experiment, and a further $\pm$ 0.24 mm due to the uneven surface of the scaling, derived from the maximum measured difference between scaling crest and vale of 0.48 mm). An approximate longitudinal wave velocity in the scaling of 7330 m s^{-1}, with 95 % confidence bounds, can be derived from the gradient in Fig. 6. This is coherent with literature values for the p-wave velocity in calcite single crystals which range from 5700 m s^{-1} to $\sim$ 7700 m s^{-1} depending on the crystal orientation [16].

Given the linear correlation of TWT to scaling thickness, a thickness resolution of 0.18 mm could be attained with the current measurement parameters.

The preliminary experiment investigating the heat transfer through the wedge yielded a temperature of 60 °C at the upper

Fig. 4 Schematic cross section of the setup with a 6.6 mm-thick scaling layer (**a**) and a 3.3 mm-thick scaling layer (**b**) with corresponding averaged A-scans at the beginning (**c**) and end (**d**) of the first descaling measurement. The green arrows mark the steel pipe backwall echoes, the red arrows mark the scaling backwall echoes. The large echoes at 25 µs and 51 µs are wedge echoes (Color figure online)
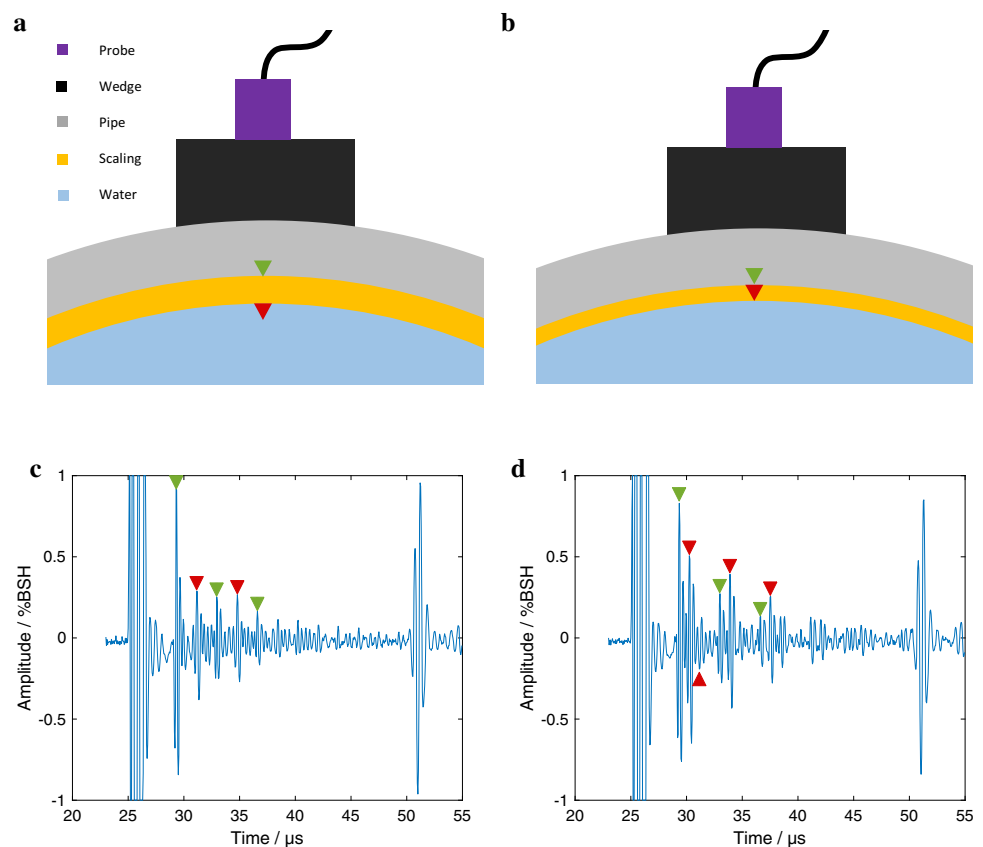
Fig. 5 Two-way travel time plotted for the first (**a**) and second (**b**) descaling measurement. The plateaus are a result of the limited time resolution of the A-scans. A-scans in (**b**) where the pipe and scaling backwall echoes were no longer distinguishable due to superposition of the wave pulses were removed
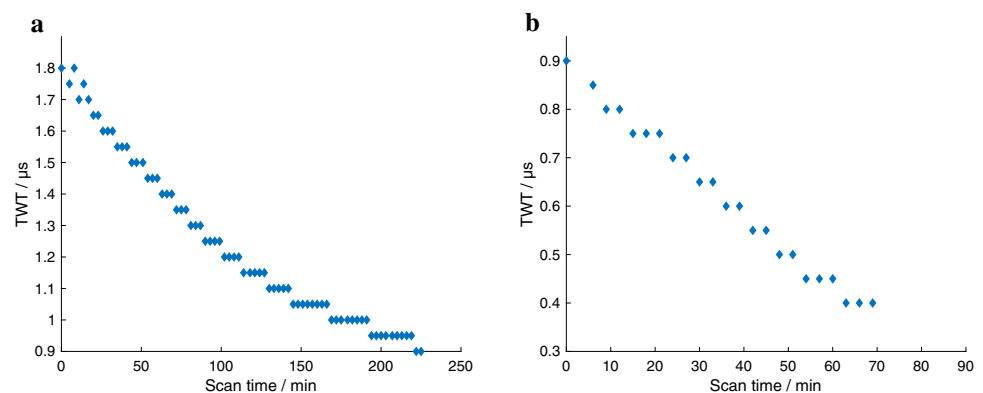
surface of the PPSU wedge, to which the ultrasound probe is coupled. A standard contact transducer has an operating temperature limit of $\sim 60\,^\circ\text{C}$ [17].

3.2 Results of Impact-Echo Measurement

Impact-echo signals for manual excitation with a $\varnothing$ 10 mm impact hammer, recorded at the beginning and end of the second descaling experiment are shown in Fig. 7a and c. 20 such signals were recorded at each time interval. These were detrended, autocorrelated, fast Fourier transformed and averaged to give frequency spectra such as those shown in Fig. 7b

and d. The corresponding frequency spectra generated using the $\varnothing$ 5 mm impact hammer are shown in Fig. 8.
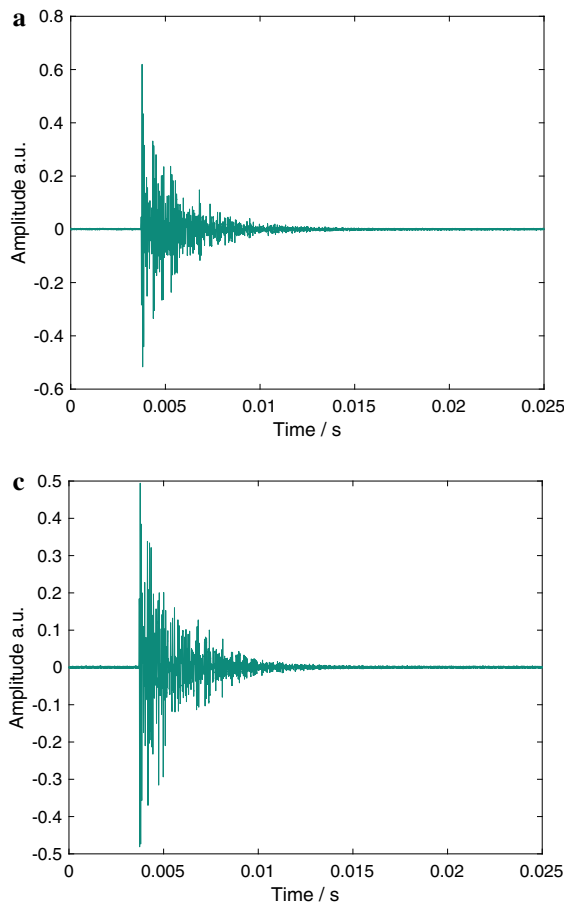
The simplest scenario for automated evaluation of the scaling thickness from the IE data would be to track the peak resonant frequency over time. This requires an informed choice of hammer. Whilst excitation with a $\varnothing$ 5 mm impact hammer, for example, showed a clear decrease in resonant frequencies (Fig. 9a, b) with scan time, the peak resonant frequency was not consistent over the course of the descaling experiment.

Excitation with a 10 mm impact hammer, on the other hand, yielded an almost continuous curve for the peak resonant frequency over the course of the descaling process
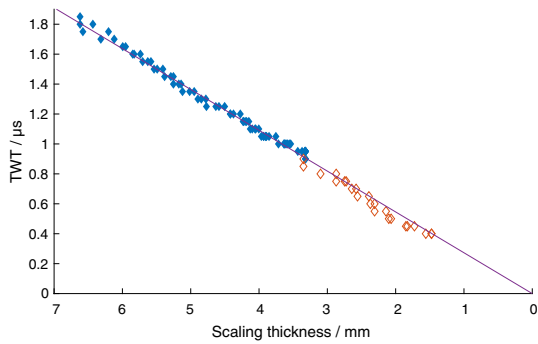
Fig. 6 TWT against mechanically measured scaling thickness for the first and second descaling experiments. The US velocity derived from the gradient is 7330 m s^{-1}. Slight corrosion of the threaded hole in the steel pipe over the course of the experiment caused outliers in the mechanically measured scaling thickness

(Fig. 10). By implementing a moving window, which successively shifts with a particular peak value in the preceding frequency spectrum, the desired frequency can be tracked,

provided it is continuous. This was done for Fig. 10. Here, the peak resonant frequency decreases with scaling thickness from an initial value of 16.6 kHz, for a (3.350 ± 0.004) mm thick scaling layer, to 15.28 kHz when no scaling is present. A linear trend is shown in the corresponding spectrogram plotted against scaling thickness (Fig. 11). With the given frequency resolution of 20 Hz, a peak frequency range of 15.28–16.6 kHz and a linear correlation between the two, a thickness resolution of (0.1 ± 0.1) mm could theoretically be reached for the scaling thickness, whereby a statistical error of 30 Hz is accounted for.

The frequency domain measured comprises modal oscillations of the pipe. As the scaling layer is etched away, the stiffness of the oscillating system decreases. A lower stiffness leads to lower resonant frequencies [18]. The mass also decreases with decreasing layer thickness, counteracting this effect, but the effect of the change in stiffness dominates [19].
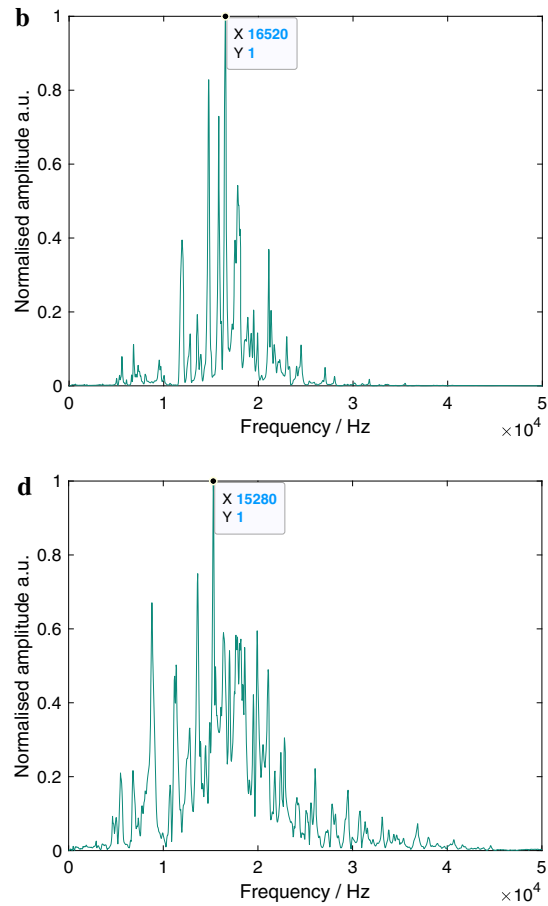

Fig. 7 **a** Signal recorded by force sensor for manual impact with a ⌀ 10 mm impact hammer at the beginning of the second descaling experiment. **b** Averaged frequency spectrum of **a** for 20 impacts. **c** Signal recorded towards the end of the second descaling experiment. **d** Averaged frequency spectrum of (**c**) for 20 impacts
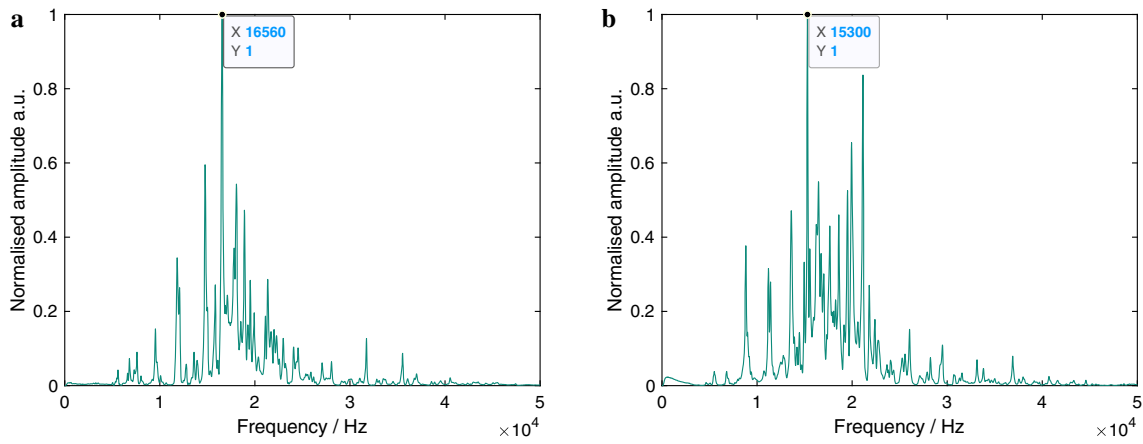
Fig. 8 **a** Averaged frequency spectrum for manual impact with a ⌀ 5 mm impact hammer at the beginning of the second descaling experiment. **b** Averaged frequency spectrum towards the end of the second descaling experiment
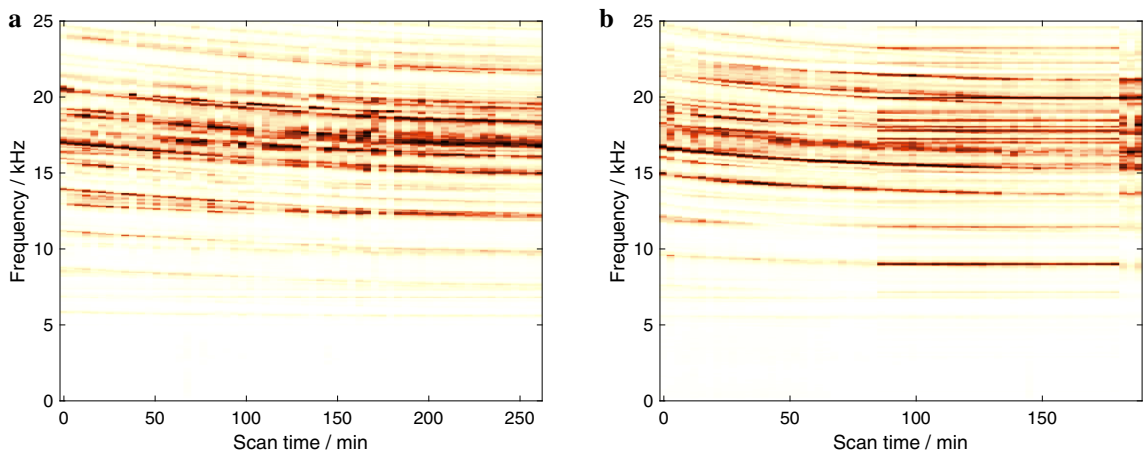
Fig. 9 Normalised frequency spectra plotted in colour scale against scan time for excitation with a ⌀ 5 mm impact hammer for the first (**a**) and second (**b**) descaling experiment
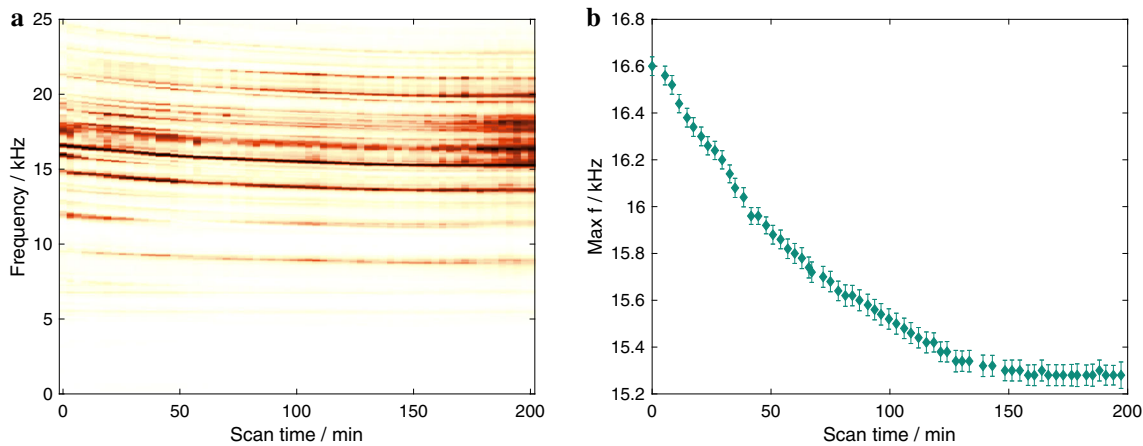
Fig. 10 Spectrogram for excitation with a ⌀ 10 mm impact hammer (**a**) and corresponding evolution of peak resonance frequency (**b**)
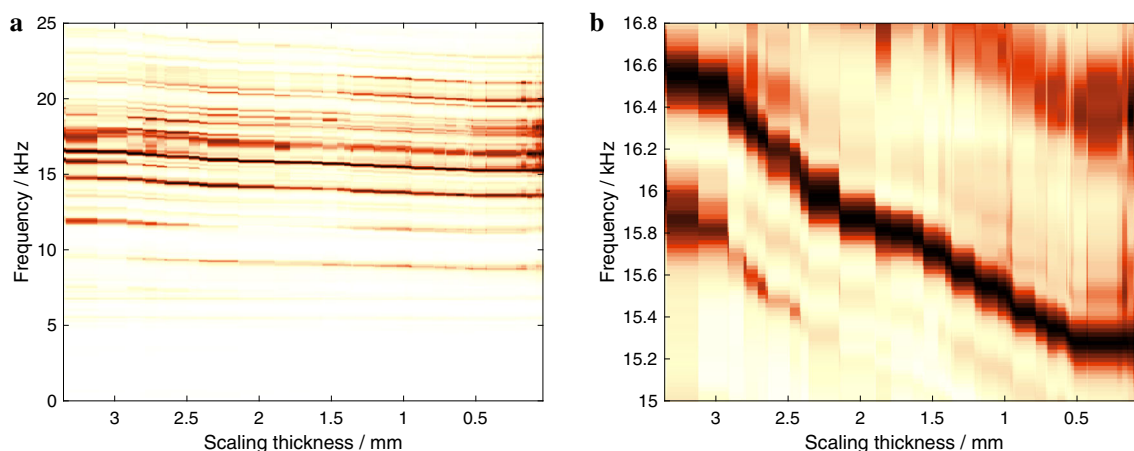
Fig. 11 a Plotted against the mechanically measured scaling thickness, the frequency spectra show a linear trend between frequency and layer thickness. Higher peak frequencies show a larger shift in frequency with layer thickness. **b** shows an outtake around the peak frequency

3.3 Calculation of the Dissolved Scaling Layer Thickness

When the RS990 was added to the scaled test rig, the protons of the acid dissolved the $CaCO_3$ and the pH increased slowly (see Fig. 12a). Since the solution was not changed during one experiment, the capacity of the acid (= free available protons) for dissolving solid $CaCO_3$ decreased and the solution became saturated. This was accompanied by a continuous increase in pH value after approx. 60 min. The electrical conductivity decreased over time (see Fig. 12b) as the protons of the acids were consumed and the dissolved $CaCO_3$ has less influence on the conductivity than H^+.

For mass balance and the back calculation of the scaling thickness, IC measurements were carried out. The mass of dissolved $CaCO_3$ during the experiment was calculated using the concentration of Ca^{2+} ions. Tables 1 and 2 show the evolution of the calcium and magnesium ion concentrations over time. Since the concentration of magnesium ions was negligible, the assumption of pure calcite scaled on the test rig is valid and in accordance with the findings of Köhl et al. [2].

Before the first experiment, a scaling layer of (6.62 ± 0.24) mm was measured by a sliding caliper. This means the amount of precipitated $CaCO_3$ on the test rig was (3.640 ± 0.018) kg (or: (1.460 ± 0.007) kg Ca^{2+}; simplification: $CaCO_3$ layer = hollow cylinder). After the first experiment, the scaling layer measured with a sliding caliper showed that (3.27 ± 0.24) mm of the $CaCO_3$ scaling were dissolved by the acidic solution. This equals to (1.770 ± 0.018) kg calcite (or (695.200 ± 7.327) g Ca^{2+}). The solution had a total volume of (40 ± 5) L, i.e. (17.380 ± 2.180) g L^{-1} Ca^{2+} should be dissolved after the first experiment. In the second experiment, (3.35 ± 0.24) mm of the scaling layer were dissolved according to the sliding caliper,

which is equivalent to (1.870 ± 0.018) g Ca^{2+}). calcite (or (734.440 ± 7.327) g Ca^{2+}) corresponding to a Ca^{2+} concentration of (18.361 ± 2.302) g L^{-1}. Although the experiments were run in succession, they should be considered as independent experiments: The set-up was openend between the experiments and the solution was exchanged.

At the end of the first experiment the measured Ca^{2+} concentration of the solution was (17.753 ± 0.065) g L^{-1}. It confirmed that half of the scaling layer was dissolved during the first experiment. At the end of the second experiment the measured Ca^{2+} concentration was (15.784 ± 0.252) g L^{-1}. The back calculation of the scaling thickness showed that during the first experiment a scaling layer of (3.294 ± 0.412) mm was dissolved which is in really good agreement with the mechanically measured dissolved scaling (3.25 ± 0.40) mm, see Fig. 13a. At the end of the second experiment a scaling thickness of (2.858 ± 0.361) mm was dissolved according to the ionic measurements (mechanical measurement: (3.33 ± 0.40) mm). Both, mechanical measurement and chemical measurement show the same development over time for the first and for the second experiment (see Fig. 13a and b respectively). With regard of the uncertainties of the experiment and measurements there is no significant difference between the measurements. Nevertheless, the mechanical measurements give a higher value for the thickness compared to the chemical measurements (see Fig. 13b), because the probe is tipping on a rough surface (see Fig. 1b), thus capturing only the peaks of the precipitates. With increasing roughness, this deviation increases. The calculated scaling layer dissolved during the experiment is shown in Tables 1 and 2.
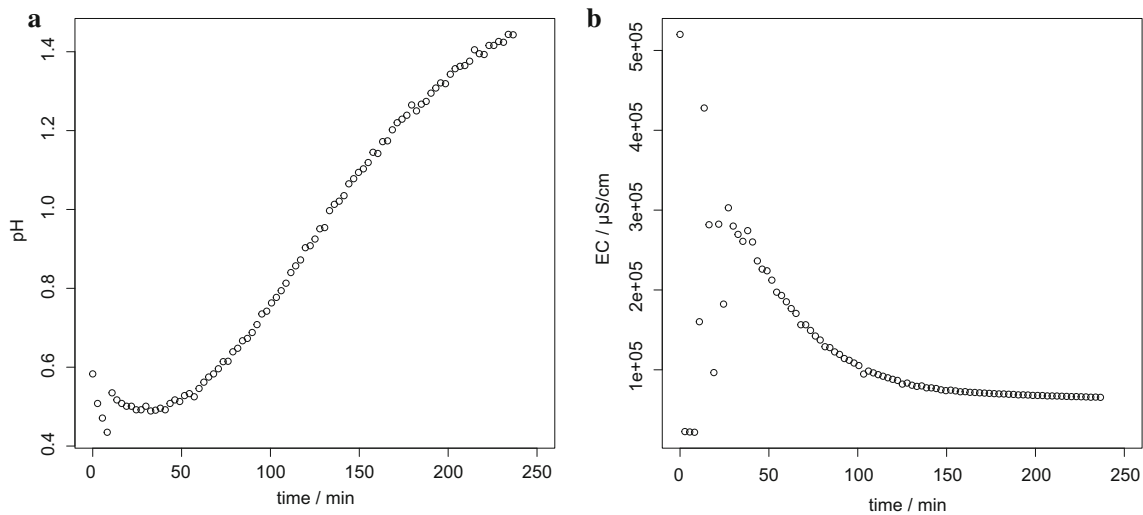
Fig. 12 Development of pH value (**a**) and electrical conductivity (EC, **b**) over the course of the first descaling experiment

Table 1 Concentration of calcium and magnesium ions (g L^{-1}, $\pm$ standard deviation) during the first experiment and the corresponding calculated thickness of the dissolved scaling layer

Time (min)	Ca^{2+} (g L^{-1})	Mg^{2+} (g L^{-1})	Dissolved scaling (calculated) (mm)
0	0.092 ± 0.682	0.130 ± 0.569	0.017 ± 0.130
3	0.585 ± 0.107	-0.024 ± 0.098	0.111 ± 0.025
9	2.343 ± 0.315	-0.001 ± 0.027	0.446 ± 0.082
15	3.089 ± 0.119	0.026 ± 0.033	0.587 ± 0.077
24	4.421 ± 0.597	0.068 ± 0.064	0.841 ± 0.155
33	5.023 ± 0.292	-0.013 ± 0.021	0.955 ± 0.132
42	6.502 ± 0.114	0.023 ± 0.013	1.225 ± 0.155
51	7.616 ± 0.178	0.066 ± 0.009	1.435 ± 0.183
60	8.842 ± 0.110	0.109 ± 0.008	1.666 ± 0.209
69	9.519 ± 0.090	0.231 ± 0.004	1.793 ± 0.225
78	10.262 ± 0.091	0.172 ± 0.028	1.933 ± 0.242
87	11.559 ± 0.048	0.277 ± 0.031	2.157 ± 0.270
96	12.383 ± 0.134	0.247 ± 0.011	2.311 ± 0.290
105	12.495 ± 1.217	0.300 ± 0.018	2.332 ± 0.370
135	14.151 ± 0.121	0.339 ± 0.005	2.641 ± 0.331
174	16.457 ± 0.326	0.430 ± 0.011	3.053 ± 0.387
207	17.753 ± 0.065	0.466 ± 0.011	3.294 ± 0.412

Table 2 Concentration of calcium and magnesium ions (g L^{-1}, $\pm$ standard deviation) during the second experiment and the corresponding calculated thickness of the dissolved scaling layer

Time (min)	Ca^{2+} (g L^{-1})	Mg^{2+} (g L^{-1})	Dissolved scaling (calculated) (mm)
0	0.111 ± 0.555	0.100 ± 0.549	0.020 ± 0.102
3	0.300 ± 0.034	-0.046 ± 0.062	0.055 ± 0.009
63	7.682 ± 1.127	0.119 ± 0.029	1.404 ± 0.271
123	13.154 ± 0.517	0.338 ± 0.045	2.382 ± 0.312
186	15.757 ± 0.083	0.379 ± 0.032	2.853 ± 0.357
203	15.784 ± 0.252	0.427 ± 0.058	2.858 ± 0.361
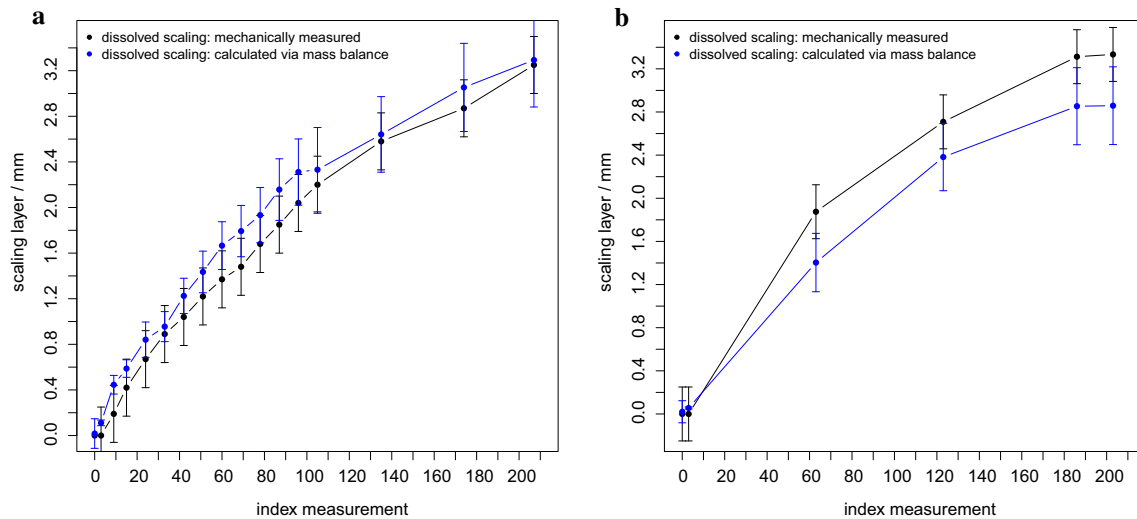
Fig. 13 Dissolved scaling layer of the first (**a**) and second (**b**) experiment: Comparison of mechanically measured (black) and calculated (blue) (Color figure online)

4 Conclusion and Discussion

Whilst both measurement techniques show potential for in-situ application, there are a number of factors which need to be considered.

For contact US testing, the prerequisites are knowledge of the longitudinal wave velocity in the pipe material as well as in the scaling; a suitably milled wedge to optimise coupling to the pipe and protect the ultrasound probe from high temperatures and access to a suitable location for the measurement apparatus. Given this information, submillimeter resolution can be reached for scaling layers thick enough for pipe and scaling echoes to be resolved. A large gain (48 dB) was necessary to make the scaling signals visible. A more inhomogeneous type of scaling (with many scattering centres) would have a lower SNR and may be more difficult to detect. The nature of the bonding between pipe and scaling is also important: Scaling signals could not be made visible in the presence of pores or cavities between pipe and scaling. Reproducibility is a further point of query which needs to be addressed: Slight shifts in coupling can effect significant changes in signal amplitude and local disbonding between pipe wall and scaling may also falsify results. Although the scaling signal is clearly visible in the experiments described, it is not necessarily detectable for other measurement constellations [20]. As the critical components (pump, heat exchangers) are typically not directly accessible, one way to determine their degree of scaling would be to model the scaling development in relevant regions of the plant and extrapolate the values of interest from local US measurements made in accessible locations nearby. Testing should be carried out in several positions to reduce susceptibility to local deviation.

For the measurement parameters described, superposition of the scaling and pipe signals for thin scaling layers limits its detectability to layers ≥ 1.5 mm. Reducing the pulse width, for example by increasing the transducer frequency, using shear wave transducers or decreasing the number of cycles, could enable the detection of thinner layers. It should be noted, however, that a higher frequency would lead to increased scattering and a reduced penetration depth [17], the attenuation of shear waves is significantly higher than that of longitudinal waves [21], whilst a shorter pulse would reduce the energy introduced into the test piece, all leading to a lower SNR. The minimum detectable scaling layer would also vary for different types of scaling: A lower US velocity would lead to an increased resolution. Geothermal power plants in the Bavarian Molasse Basin mostly implement preventive measures such as reducing the temperature of the thermal water from the production well by some degrees or injecting carbon dioxide to counteract limescale [22,23]. Layer thicknesses of ≥ 1.5 mm are therefore rare on the production side of the plant. The injection well, on the other hand, can have scaling layers on the order of 1 cm, and could be an interesting monitoring location. Improved measureability might be achieved by comparison to simulation results or using machine learning algorithms but this requires further research.

Theoretically, an air-coupled ultrasonic testing setup would also withstand the high temperature of geothermal pipe surfaces. Due to the high impedance mismatch between air and steel, however, the signal amplitude introduced into the specimen would be negligible ($\sim 0.001\%$) [24]. This would result in a very low SNR. Another interesting approach would be phased array ultrasonic testing with full matrix capture (FMC) acquisition and post-processing, for example

using the total focusing method (TFM) for maximal resolution. This was also tested and has comparable limitations to single element contact UT, but is more expensive (financially as well as computationally) and the probe introduces less energy into the specimen: without TFM post-processing the scaling signal could not be observed at all.

The correlation of the obtained signals to scaling layer thickness could be validated by the back calculation of the dissolved scaling layer via the measured Ca^{2+} ion concentration of the solution: the calculation only deviates by 1.35% for the first and by 14.26% for the second experiment from the mechanical measurement and shows the same development over time as the contact US and IE measurements. It makes sense that the deviation between the mechanical and chemical measurement of the second experiment exceeds that of the first experiment as the play in the threaded hole caused by acid corrosion increased over the course of the experiments. Furthermore, due to the probe tipping on the rough surface of the scaling, only the peaks of the precipitates are detected, which is why the mechanically measured scaling thickness should generally slightly exceed the one calculated via the Ca^{2+} ion concentration of the solution (see also Figs. 1b, 13b). With increasing roughness, the deviation also increases.

A scaling monitoring using IE could resolve much thinner scaling layers. It does, however, need a calibration of the system, correlating a given pipe geometry and scaling type to the corresponding frequency spectrum. For in-situ measurements this will involve recording signals and creating a reference spectrogram for the geothermal power plant in question during one revision cycle. The frequency spectrum recorded at the beginning of such a cycle, so directly after cleaning, will correspond to a bare pipe with no scaling. The frequency spectrum at the end of the cycle can be attributed to the corresponding scaling thickness determined via mechanical measurement provided the pipe can be opened at this time. For future determination of scaling thickness the frequency spectrum at a given time can be correlated via linear regression to this reference spectrogram.

The length of the pipe segment studied in this work was chosen for practiacl reasons (weight and manoeuvrability). The resonance frequencies would be expected to decrease with increasing ratio of pipe length to outer radius, whereby the amount by which a resonance frequency decreases varies depending on vibration mode [19,25]. It can be seen in the spectrograms presented, that the majority of peaks exhibit a consistently decreasing trend with reduced scaling thickness. The occurence of the maximum peak, however, may be affected by a number of factors, such as the excited frequency range (dependent on contact time, diameter of impact hammer) [26], in-situ boundary conditions, impedance ratio of pipe to scaling and differences in attenuation depending on material properties and vibration mode [27]. Furthermore, lower frequencies shift less than higher frequencies with scaling layer thickness. The dependency of frequency shift on frequency is yet to be determined (a simulation to this end is currently in progress). Nevertheless, once a specific peak, or peak group is chosen as the indicator for scaling thickness, based on parametric studies, the described method can be effectively applied.

For optimal excitation (where a peak resonant frequency can simply be tracked over time), a suitable hammer size/material and impact energy have to be established. Automation of the excitation using a solenoid-based impactor is currently being tested. Increasing the frequency resolution could further improve accuracy.

Laser excitation presents an alternative broadband, contact-free means of excitation [28,29], but comes with higher costs and extensive safety regulations.

Provided a calibration of the measuring apparatus can be carried out, UT and IE have a comparable resolution and are relatively inexpensive and simple to implement. The limiting factor for contact UT is the minimum scaling layer thickness which can be detected, the ultrasound properties of the scaling and optimal coupling for a usable SNR. That of IE testing is the calibration needed to evaluate the results. Combining data from contact UT and IE testing could improve resolution and the reliability of the diagnosis. The next steps towards a reliable scaling monitoring will involve a more detailed analysis of the effect of temperature and comparison to simulation results.

Author Contributions IS, LZ and CG participated in the conception and design of this research and its experiments; IS carried out the design and interpretation of the ultrasound and impact-echo data; LZ carried out the design and interpretation of the IC measurements; IS and LZ performed the respective experiments and analysis; IS wrote the original draft, LZ wrote Chapter 3.3 and contributed to Chapter 4; IS, LZ and CG participated in the revisions of the manuscript. All authors read and approved the final manuscript.

Data Availability Not applicable.

Declarations

Competing interests The authors declare that they have no conflict of interest.

Ethical Approval and Consent to Participate Not applicable.

Consent for Publication Not applicable.

Authors' Information Not applicable.

References

1. Boch, R., Leis, A., Haslinger, E., Goldbrunner, J.E., Mittermayr, F., Fröschl, H., Hippler, D., Dietzel, M.: Scale-fragment formation impairing geothermal energy production: interacting h 2 s corrosion and CACO 3 crystal growth. Geotherm. Energy **5**(1), 1–19 (2017)
2. Köhl, B., Elsner, M., Baumann, T.: Hydrochemical and operational parameters driving carbonate scale kinetics at geothermal facilities in the Bavarian molasse basin. Geotherm. Energy **8**(1), 1–30 (2020)
3. Rostron, P.: Critical review of pipeline scale measurement technologies. Indian J. Sci. Technol. **11**(17), 1–18 (2018)
4. Bertani, R.: Geothermal power generation in the world 2010–2014 update report. Geothermics **60**, 31–43 (2016)
5. Köhl, B., Grundy, J., Baumann, T.: Rippled scales in a geothermal facility in the Bavarian molasse basin: a key to understand the calcite scaling process. Geotherm. Energy **8**(1), 1–27 (2020)
6. Feasey, N.D., Freiter, E., Jordan, M., Wintle, R.: Field experiences with a novel near real time monitor for scale deposition in oilfield systems. In: Corrosion 2000 (2000). OnePetro
7. Okazaki, T., Imai, K., Tan, S.Y., Yong, Y.T., Rahman, F.A., Hata, N., Taguchi, S., Ueda, A., Kuramitz, H.: Fundamental study on the development of fiber optic sensor for real-time sensing of $CaCO_3$ scale formation in geothermal water. Anal. Sci. **31**(3), 177–183 (2015)
8. Reed, C., Robinson, A.J., Smart, D.: Techniques for Monitoring Structural Behaviour of Pipeline Systems. American Water Works Association, Denver (2004)
9. Coletti, F., Crittenden, B.D., Haslam, A.J., Hewitt, G.F., Jackson, G., Jimenez-Serratos, G., Macchietto, S., Matar, O.K., Müller, E.A., Sileri, D., et al.: Modeling of fouling from molecular to plant scale. In: Crude Oil Fouling, pp. 179–320. Elsevier, Amsterdam (2015)
10. Wallhäußer, E., Hussein, M., Becker, T.: Detection methods of fouling in heat exchangers in the food industry. Food Control **27**(1), 1–10 (2012)
11. Kažys, R., Voleišis, A., Voleišienė, B.: High temperature ultrasonic transducers. Ultragarsas. Ultrasound **63**(2), 7–17 (2008)
12. Carino, N.J.: The impact-echo method: an overview. Structures 2001: A Structural Engineering Odyssey, 1–18 (2001)
13. Grosse, C., Jüngert, A., Jatzlau, P.: Local acoustic resonance spectroscopy (2018)
14. Gibson, A., Popovics, J.S.: Lamb wave basis for impact-echo method analysis. J. Eng. Mech. **131**(4), 438–443 (2005)
15. Baggens, O., Ryden, N.: Lamb wave plate parameters from combined impact-echo and surface wave measurement. In: Proceedings of the International Symposium NDT in Civil Engineering, vol. 1517. Berlin, Germany (2015)
16. Rüdrich, J.M.: Gefügekontrollierte verwitterung natürlicher und konservierter marmore (2003)
17. Krautkrämer, J., Krautkrämer, H.: Werkstoffprüfung Mit Ultraschall. Springer, Heidelberg (2013)
18. Brincker, R., Ventura, C.: Introduction to Operational Modal Analysis. Wiley, Chichester (2015)
19. Zhou, D., Cheung, Y., Lo, S., Au, F.: 3d vibration analysis of solid and hollow circular cylinders via Chebyshev-Ritz method. Comput. Methods Appl. Mech. Eng. **192**(13–14), 1575–1589 (2003)
20. Gunarathne, G., Keatch, R.: Novel techniques for monitoring and enhancing dissolution of mineral deposits in petroleum pipelines. Ultrasonics **34**(2–5), 411–419 (1996)
21. Ono, K.: Dynamic viscosity and transverse ultrasonic attenuation of engineering materials. Appl. Sci. **10**(15), 5265 (2020)
22. Koch, M., Ruck, W.: Injection of CO_2 for the inhibition of scaling in ATES systems. Technical report, SAE Technical Paper (1992)
23. Irl, M., Aubele, K., Baumann, T., Dawo, F., Hindelang, J., Keim, M., Mayer-Ullmann, P., Molar-Cruz, A., Walcher, F., Wieland, C., et al.: Flexibilitätsoptionen der strom-und wärmeerzeugung mit geothermie in einem von volatilem stromangebot bestimmten energiesystem (2020)
24. Regtien, P., Dertien, E.: Acoustic Sensors. Sensors for Mechatronics, 2nd edn., pp. 267–303. Elsevier, Amsterdam (2018)
25. Lin, S.: Coupled vibration of isotropic metal hollow cylinders with large geometrical dimensions. J. Sound Vib. **305**(1–2), 308–316 (2007)
26. Carino, N.J.: Impact echo: the fundamentals. In: Proceedings of the International Symposium Non-Destructive Testing in Civil Engineering (NDT-CE), pp. 15–17. Berlin, Germany (2015)
27. Ono, K.: Experimental determination of lamb-wave attenuation coefficients. Appl. Sci. **12**(13), 6735 (2022)
28. Pétillon, O., Dupuis, J., David, D., Voillaume, H., Trétout, H.: Laser ultrasonics: a non contacting NDT system. In: Review of Progress in Quantitative Nondestructive Evaluation, pp. 1189–1195. Springer, Iowa (1995)
29. Brauns, M., Lucking, F., Fischer, B., Thomson, C., Ivakhnenko, I.: Laser-excited acoustics for contact-free inspection of aerospace composites. Mater. Eval. **79**(1), 28–37 (2021)